buildings

MDPI

Article

Stability Study of Bridge Piles Subject to Construction Activities and Channel Excavation in Deep Soft Soil Areas

Wanpeng Ding [1], Shengnian Wang [1,2,*], Guoxu Wang [1], Wentao Hu [1] and Jian Liu [1]

[1] College of Transportation Science and Engineering, Nanjing Tech University, Nanjing 211816, China
[2] Jiangsu Province Engineering Research Center of Transportation Infrastructure Security Technology, Nanjing 211816, China
* Correspondence: shengnian.wang@njtech.edu.cn

Abstract

Pile foundations are critical load-bearing components in bridge structures, particularly in soft, high-moisture soils susceptible to external disturbances. This study investigated the impact of large-scale soil excavation on the stability of adjacent pile foundations through comprehensive field monitoring of a newly constructed bridge during both the bridge construction and channel excavation phases. The close proximity of the excavation site to the pile caps facilitated a detailed assessment of soil–structure interaction. The results indicate that the pile axial force peaked at the pile head and decreased progressively with depth, consistent with the load transfer mechanism of friction piles. Notably, a distinct variation in axial force was observed at the bedrock interface, attributed to reduced relative displacement between the pile and the surrounding soil. Furthermore, channel water filling raised the local groundwater table, which increased the buoyancy and reduced negative skin friction, thereby decreasing the pile axial force. The study also highlighted the sensitivity of pile deformation in soft soil to unbalanced earth pressure. Asymmetric excavation and surface surcharge loading were identified as critical factors compromising pile stability and overall structural safety. These findings provide valuable insights for construction practices and offer effective strategies to mitigate adverse excavation effects, ensuring long-term structural stability.

Keywords: bridge construction; bridge pile foundation; channel excavation; field monitoring; soft soil sites

Check for updates

Academic Editor: Eugeniusz Koda

Received: 8 December 2025
Revised: 9 January 2026
Accepted: 14 January 2026
Published: 16 January 2026

Copyright: © 2026 by the authors. Licensee MDPI, Basel, Switzerland. This article is an open access article distributed under the terms and conditions of the Creative Commons Attribution (CC BY) license.

1. Introduction

As the primary load-bearing component of a bridge, the pile foundation is essential for transferring loads from the superstructure and vehicular traffic to the underlying soil. The stability of the pile foundation is paramount for ensuring the structural integrity and long-term performance of the bridge. Driven by rapid global economic expansion, existing infrastructure is increasingly insufficient to meet societal demands, necessitating the development of new infrastructure projects. However, the construction of such projects often involves extensive soil excavation, which can significantly undermine the stability of adjacent structures [1–4]. Specifically, when excavation activities are conducted near a bridge, the resulting soil disturbances can lead to changes in stress distribution and deformation patterns within the pile foundations, potentially compromising the stability of the bridge structure. These effects are particularly pronounced in regions characterized by deep soft soil, where pile foundations are extensively embedded to support the imposed

loads. The inherent properties of soft soil, such as high moisture content and high plasticity, further exacerbate the impact of excavation on pile foundations, thereby amplifying the associated risks [5–11].

Extensive research has demonstrated that soil excavation disturbances can significantly compromise the safety and functionality of nearby structures [12–16]. These impacts are particularly pronounced for pile foundations, which are highly susceptible to soil disturbances due to the critical role of pile–soil interaction in load transfer [17–19]. To better understand soil–pile interactions, an analytical method was proposed based on drained solutions for cavity expansion and contraction in a unified clay and sand model. This approach has been effectively utilized to evaluate the effects of tunnel excavation on pile foundation performance [20]. In addition, the improved Poulos method and three-dimensional centrifuge tests were employed to investigate pile–soil interactions during tunnel excavation. Findings suggested that the proximity of a tunnel excavation to both the ground surface and the pile significantly amplifies its impact on the pile foundation stability [21,22]. Liu et al. [23] developed a specialized test device to simulate actual pile loading conditions, enabling a detailed analysis of excavation effects on supporting piles. Excavation in soft soil areas poses even greater challenges due to the inherently poor engineering properties of these soils [24–28]. Numerous studies have focused on understanding the influence of soil excavation on structures in soft soil regions. By employing the hyperbolic model and field monitoring techniques, researchers analyzed the variations in pile side friction, pile tip resistance, and soil movement caused by excavation. A predictive framework was subsequently developed to estimate pile responses to adjacent excavations, which has been validated through real-world case studies [29,30]. Furthermore, Choosrithong and Schweiger [31] investigated the effect of embedded depth on strut failures induced by excavation using finite element modeling techniques.

Field monitoring is a pivotal approach for assessing the impacts of soil excavation on pile foundations. Empirical data from field studies indicate that the deformation behavior of retaining structures is significantly influenced by deep foundation pit excavation. Research demonstrates that optimizing the excavation process can effectively reduce adverse interactions between adjacent foundation pits [32]. During foundation pit excavation, field monitoring has captured considerable lateral deformation and settlement in retaining walls and the surrounding soil, with bridge piles also experiencing pronounced settlement. Finite element analysis attributed this excessive settlement primarily to pore water loss in the soil during the excavation [33]. To address this issue, a soil damage model was developed that leverages field monitoring data to calculate surface settlement induced by excavation. Subsequent simulations confirmed that increasing pile diameter is an effective measure for reducing pile foundation settlement [34,35]. Furthermore, advancements in monitoring technologies have significantly improved the accuracy and reliability of pile foundation analysis. For instance, the utilization of optical leveling lines has yielded more precise and consistent data for monitoring settlement [36,37]. Conventionally, strain gauges integrated into steel reinforcement cages monitor strain development within piles, offering critical insights into load transfer mechanisms [38]. Similarly, Nguyen et al. [39] employed pressure cells at the pile heads to measure the loads acting on pile foundations. Chen et al. [40] developed an advanced multi-scale monitoring system for deep-water settlement in super-large pile groups, integrating high-precision micro-pressure sensors, static water level gauges, and settlement analysis instruments. This innovative system has been successfully implemented to monitor settlement in bridge pile foundations, demonstrating its practical applicability. These findings highlight the indispensable role of field monitoring in understanding and mitigating the impacts of excavation on pile foundations. Recent advancements in optical fiber technology have further transformed pile foundation mon-

itoring. Fiber Bragg grating sensors were attached to steel reinforcement cages to track strain development in pile foundations and rectangular pile walls, providing high-precision measurements [41,42]. Distributed optical fiber sensors have also been utilized to monitor stress and deformation in bridge pile foundations during construction, delivering detailed data on structural performance [43,44]. Additionally, distributed optical fiber strain sensors have been employed to investigate stress variations at the pile–soil interface caused by tunnel excavation, contributing to a deeper understanding of soil–structure interactions [45]. However, despite advantages such as continuous, real-time monitoring, their widespread adoption is hindered by higher costs and sensitivity to factors like fiber length and quality. Consequently, selecting an appropriate monitoring method for pile foundations necessitates a thorough evaluation of the specific monitoring objectives, budgetary constraints, accuracy requirements, and other relevant parameters.

Existing field monitoring studies on the effects of soil excavation on adjacent pile foundations have primarily focused on activities associated with foundation pits, tunnels, and subway stations [46,47]. However, there is a scarcity of research addressing the impact of large-scale soil excavation on bridge pile foundations in deep soft soil regions. Specifically, case studies involving excavations proximal to the pile cap, where soil-structure interaction risks are significantly amplified, are particularly rare. In this study, the entire process of bridge construction and channel excavation was comprehensively monitored, with a specific focus on the behavior of bridge pile foundations. Key parameters, including axial force evolution, pile inclination, and pier displacement, were systematically analyzed. The findings provide critical insights into the response of pile foundations to large-scale excavation in soft soil, offering valuable guidance for the design and construction of bridges in such complex geotechnical environments.

2. Channel Project and Site Conditions

The new channel project is located in Haining City, Zhejiang Province, China. It is designed with a navigational clearance height of 7.0 m and a maximum navigable water level of 2.4 m. The channel passes underneath seven bridges. Among these, one bridge is significantly affected by soil excavation due to the proximity of its pier to the excavation area. This specific bridge is highlighted in yellow in Figure 1. At this location, the channel excavation has a width of 70 m and a depth of 8 m, with the ground elevation corresponding to the top of the pile cap. The monitored bridge is a continuous variable-section box girder structure. Its pile cap measures 34.5 m in length, 7.5 m in width, and 2.5 m in height. The foundation system consists of 16 drilled cast-in-place piles, each with a length of 80 m and a diameter of 1.8 m. The new channel intersects the main span of the bridge, creating a complex interaction between the excavation and the bridge structure. The spatial relationship between the channel and the bridge is depicted in Figure 1.

The project site is situated within the Hangjiahu alluvial-lacustrine plain, characterized by significant deposits of soft soil. At the bridge location, the soft soil layer reaches a maximum thickness of approximately 45 m. Table 1 summarizes the in situ subsurface conditions, including layer thicknesses and detailed soil properties obtained from both field investigation and laboratory testing.

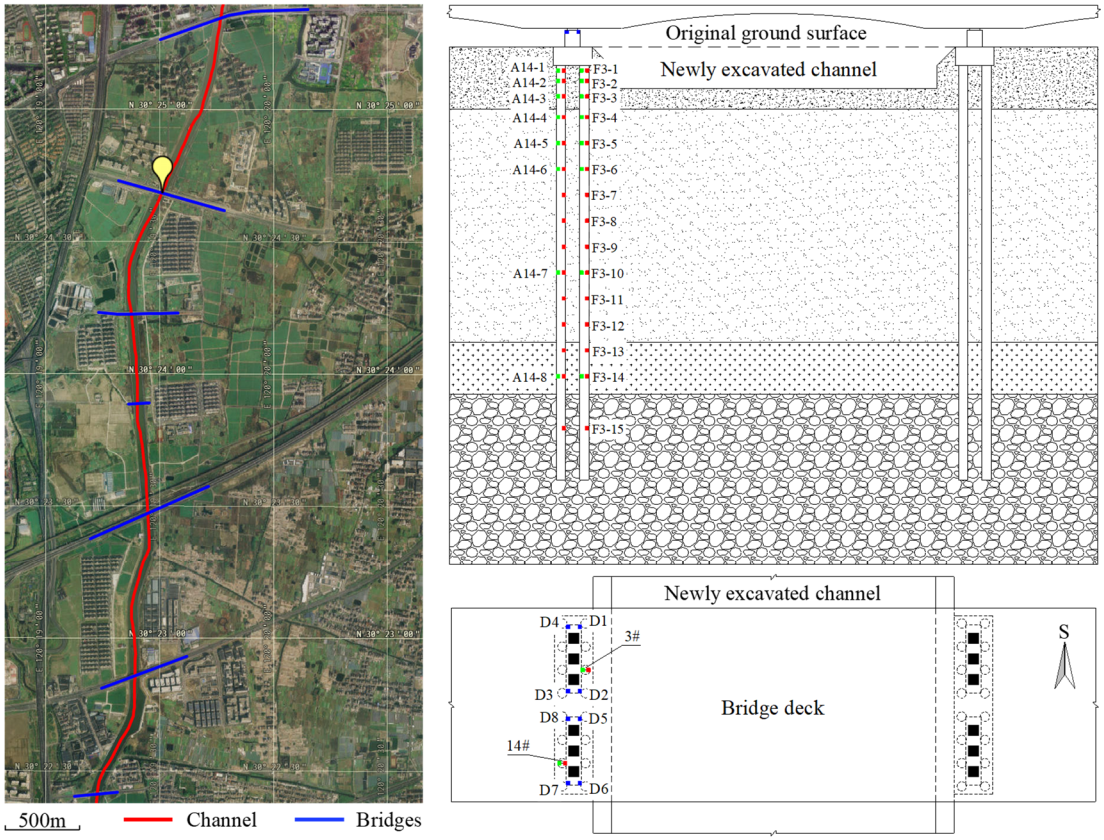


Figure 1. Relative position of the bridge and channel and layout of measurement points.

Table 1. Soil layer information.

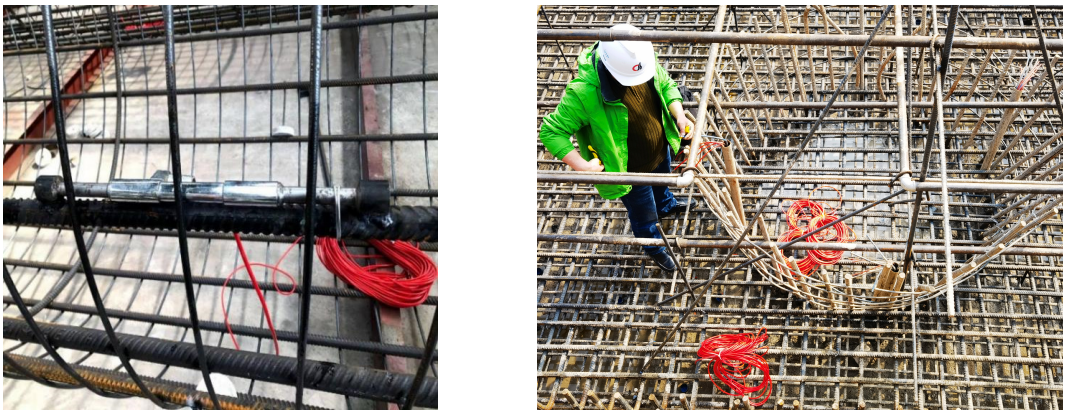
Soil Type	P (kg/m^3)	c/kPa	φ/°	E/MPa	μ	H/m
Silty clay	1850	22.5	18.6	17.3	0.36	12
Muddy clay	1730	12.8	9.2	7.3	0.48	45
Silt	1900	16.0	22.6	24.0	0.34	10
Moderately weathered bedrock	2400	30.0	35.0	42.0	0.36	33

3. Field Measure

During bridge construction and soil excavation, surface and ground displacements can be readily measured due to their accessibility. However, acquiring field data for buried structural elements, such as pile foundations, poses considerable challenges. To address this, sensors embedded within the structure are commonly employed for monitoring. This approach is widely regarded as reliable, efficient, making it a practical solution for assessing the behavior of subsurface structures under varying load and displacement conditions.

To evaluate the effects of bridge construction and soil excavation on pile foundations, a comprehensive monitoring program was implemented to measure axial force, tilt angle, and pier displacement with a frequency of once daily. Two piles (designated as 3# and 14#) beneath the same pier were selected as the study objects—one located adjacent to the channel and the other positioned farther away. Axial forces within the piles were monitored using rebar stress meters affixed to the reinforcement cages. These sensors had a measurement range of −160 MPa to 250 MPa, with an accuracy of 0.2 MPa; they were calibrated to record tensile stress as negative values and compressive stress as positive values. The sensors were securely mounted onto the steel reinforcement bars, as illustrated in Figure 2. Axial force measurement points were established at 15 depths along each pile:

F3-1 to F3-15 for pile 3# and F14-1 to F14-15 for pile 14#. These measurement points were strategically distributed at pile depths of 1 m, 3 m, 6 m, 10 m, 15 m, 20 m, 25 m, 30 m, 35 m, 40 m, 45 m, 50 m, 55 m, 60 m, and 70 m, as depicted in Figure 1. This configuration enabled a detailed assessment of the pile response under varying conditions induced by construction activities and soil excavation, providing critical insights into the behavior of pile foundations in deep soft soil environments.



(**a**) (**b**)

Figure 2. Field installation of the monitoring sensors: (**a**) Steel bar stress sensor; (**b**) Fixation of the sensor on the reinforcement cage.

Additionally, inclinometers were installed on the reinforcement cages to monitor the inclination angle and direction of the piles, as illustrated in Figure 3. These inclinometers were configured to measure inclination changes along two mutually perpendicular axes, X and Y. In the X direction, positive values indicate a tilt away from the channel, while negative values indicate a tilt toward the channel. Similarly, in the Y direction, positive values denote a tilt to the south, and negative values represent a tilt to the north. The inclinometers had a measurement range of -30° to 30°, with an accuracy of 0.03°, ensuring high-precision monitoring of pile inclination. Measurement points were designated as A3-1 to A3-8 for pile 3# and A14-1 to A14-8 for pile 14#, distributed at pile depths of 1 m, 3 m, 6 m, 10 m, 15 m, 20 m, 40 m, and 60 m, as depicted in Figure 1. To enhance data reliability and ensure the durability of the monitoring system, the lead wires from both the steel bar stress sensors and inclinometers were encased in protective plastic tubes and securely connected to the data acquisition system.

To monitor the displacement of the bridge pier, inclinometer sensors were installed at the four corners of the pier. These sensors were securely mounted using steel angle brackets, ensuring accurate inclination measurement at each corner. The inclinometers had a measurement range of -30° to 30°, with an accuracy of 0.1°, allowing for comprehensive monitoring of tilt variations. Pier displacement was calculated by analyzing the recorded inclination data. The sensor layout is illustrated in Figure 4, with the pier displacement measurement points designated as D1 through D8. The precise locations of these measurement points are depicted in Figure 1, providing a clear and comprehensive reference for the monitoring configuration.



(**a**) (**b**)

Figure 3. Field installation of the monitoring sensors: (**a**) Installation of the inclinometer; (**b**) Protection and arrangement of data transmission cables on the pile cap.



(**a**) (**b**)

Figure 4. Field installation of the monitoring sensors: (**a**) Inclination sensor on bridge pier; (**b**) The data acquisition unit mounted on the bridge pier.

4. Monitoring Results

Monitoring of axial force and inclination angle of the piles was initiated in late April 2021, subsequent to the completion of the pile foundation construction. Pier displacement monitoring commenced in September 2021, following the completion of the bridge pier construction. The data collected for each monitoring parameter are systematically presented and analyzed in the following sections.

4.1. Monitoring Data of Pile Shaft Axial Force

During the foundation construction, some monitoring equipment was inevitably damaged, resulting in the loss of some monitoring data. Nevertheless, the remaining axial force monitoring data, as shown in Figure 5, provide valuable insights into the behavior of the pile foundations. For pile 3#, the axial force exhibited a progressive increase during the construction of the superstructure, eventually stabilizing after the superstructure was completed and closure was achieved in December 2021. Notably, the axial force at F3-2 continued to rise, attributed to the combined effects of increased superstructure loads and pile–soil interaction. The axial force distribution along pile 3# after the completion of bridge construction can be categorized into three distinct intervals. The axial force at F3-2 stabi-

lized at approximately 2900 kN, while the forces at F3-3, F3-6, and F3-7 stabilized at around 1300 kN. In contrast, the axial forces at F3-10, F3-11, F3-12, and F3-13 stabilized at approximately 500 kN. The axial force of pile 3# decreased progressively with depth, aligning with the load transfer mechanism of friction piles. Similarly, pile 14# demonstrated an increase in axial force during the superstructure construction, with stabilization observed after the superstructure was completed. However, unlike pile 3#, the maximum axial force for pile 14# occurred at F14-15, located at a depth of 70 m. This corresponds to the rock-socketed section of the pile foundation.

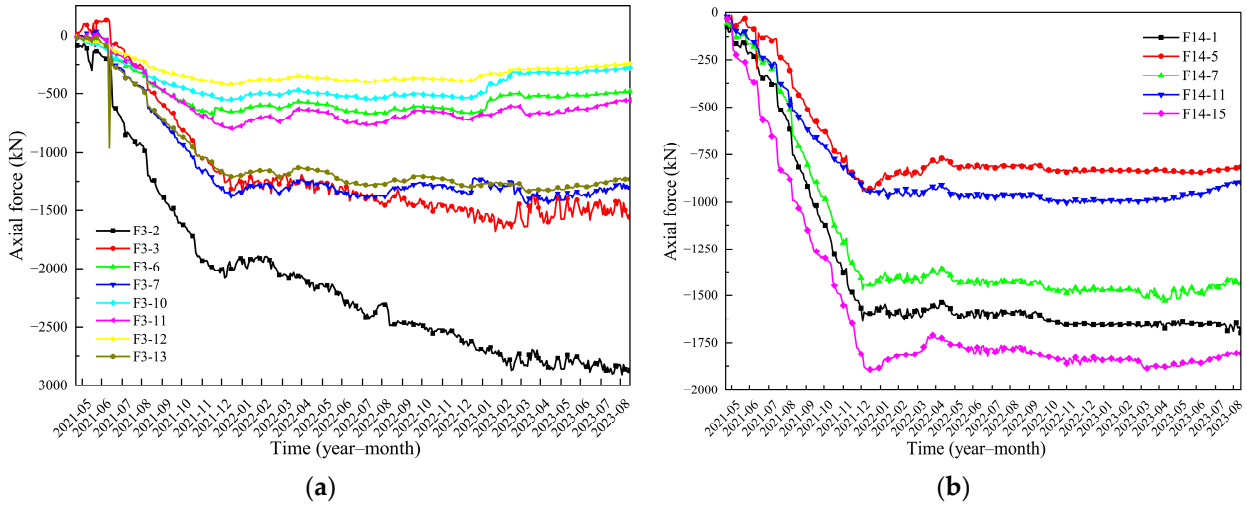


Figure 5. Monitoring data of axial force: (**a**) Monitoring data of axial force of pile 3#; (**b**) Monitoring data of axial force of pile 14#.

4.2. Monitoring Data of Pile Inclination Angle

During field monitoring, data from monitoring points A3-3 and A14-2 were lost due to damage caused by external loads. However, reliable and consistent data were obtained from the remaining monitoring points, ensuring the integrity of the overall dataset. During the initial stages of construction, the X-direction inclination angle of pile 3# at monitoring point A3-7 exhibited a slight tilt toward the channel. However, as construction progressed, the inclination direction reversed, with the pile rapidly tilting away from the channel. This shift reached a maximum recorded inclination angle of 0.35°. Between May and July 2021, monitoring points A3-2, A3-1, A3-6, and A3-4 also showed a progressive tilt away from the channel, indicating a consistent displacement trend in response to construction activities. Conversely, monitoring points A3-5 and A3-8 displayed negligible inclination throughout the monitoring period, suggesting minimal influence from the construction and excavation processes. These observations are illustrated in Figure 6a. Regarding the Y-direction inclination angle of pile 3#, as shown in Figure 6b, monitoring point A3-2 initially exhibited a southward inclination. Throughout the construction period, the inclination angle of A3-2 increased progressively. Between May and June 2021, monitoring points A3-1, A3-4, and A3-6 also exhibited a southward tilt, after which their inclination angles remained relatively stable. In comparison, A3-7 displayed a minor initial northward tilt, which was followed by a rapid tilt toward the south. Similarly, A3-5 demonstrated a slight southward inclination during the later stages of construction. Notably, A3-8 showed negligible inclination throughout the entire construction process, indicating negligible displacement in the Y-direction.

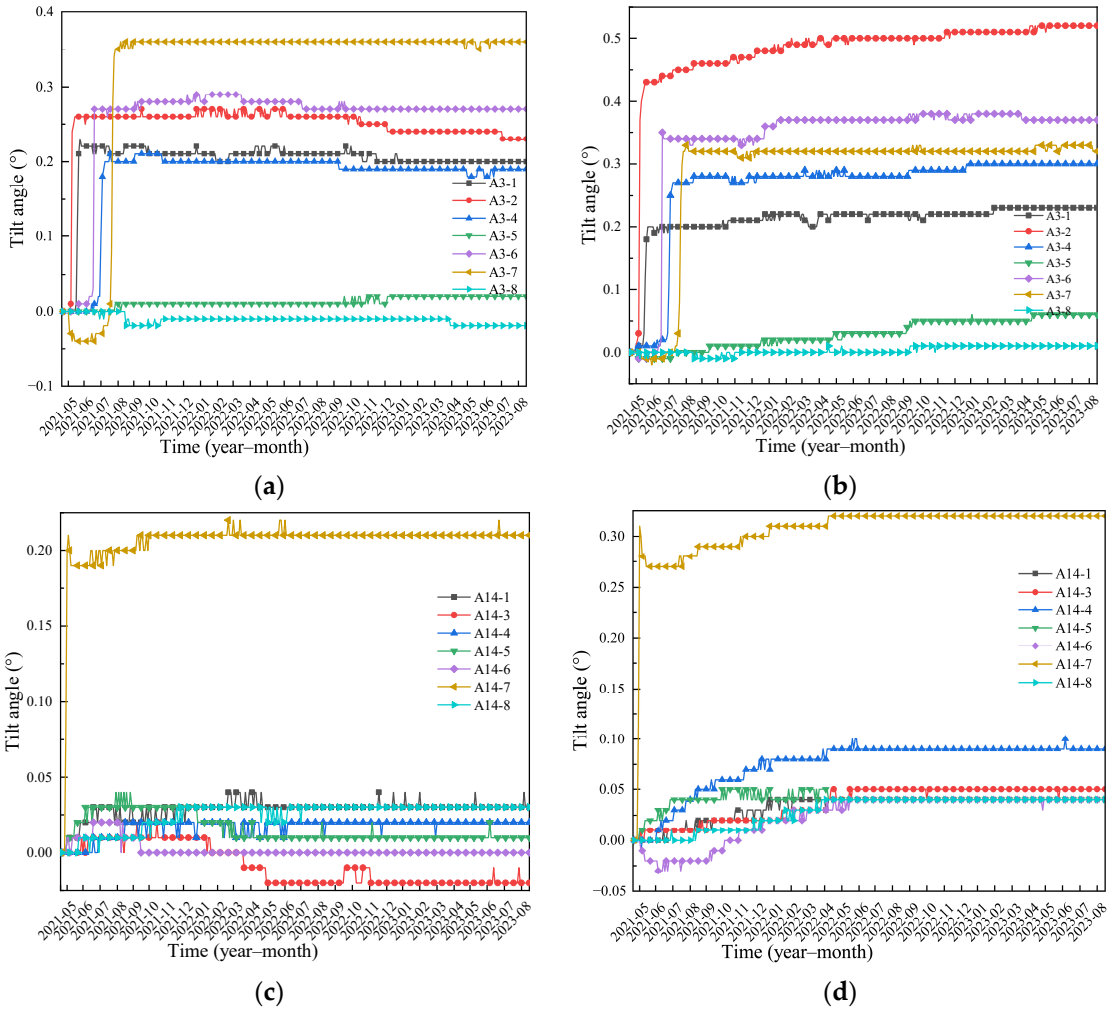


Figure 6. Monitoring data of inclination angle: (**a**) Inclination angle in X direction of pile 3#; (**b**) Inclination angle in Y direction of pile 3#; (**c**) Inclination angle in X direction of pile 14#; (**d**) Inclination angle in Y direction of pile 14#.

For pile 14#, the X-direction inclination at monitoring point A14-7 exhibited a rapid increase during the initial construction phase, with the pile tilting away from the channel. This inclination eventually stabilized at approximately 0.21°. Conversely, the inclination angles recorded at other monitoring points remained negligible, with all values maintaining below 0.05°, as depicted in Figure 6c. The Y-direction inclination angle of pile 14#, as shown in Figure 6d, exhibited a trend consistent with that observed in the X-direction. Specifically, the inclination angle at monitoring point A14-7 increased concurrently with its X-direction counterpart, eventually stabilizing at approximately 0.32°. Monitoring points A14-1, A14-3, A14-4, A14-5, and A14-8 displayed a gradual increase, correlating with the progressive loading of the superstructure. These points stabilized upon the completion of the superstructure. In contrast, A14-6 displayed an initial northward tilt during the early stages of construction, which subsequently shifted to a southward inclination as construction progressed.

4.3. Monitoring Data of Bridge Pier Displacement

According to the displacement monitoring data collected for the pier, monitoring point D5 exhibited the highest recorded displacement during the entire construction period. Due to space limitations, only the displacement data for D5 are presented in this analysis. Initial measurements taken with a total station at the time of inclination sensor installation

indicated that the pier had an initial displacement of 0.9 mm. Throughout October 2021, the displacement of D5 showed a progressive increase toward the channel side, reaching a maximum value of 12.5 mm on October 24. Following this peak, the displacement trend reversed, displaying a gradual decline, as illustrated in Figure 7.

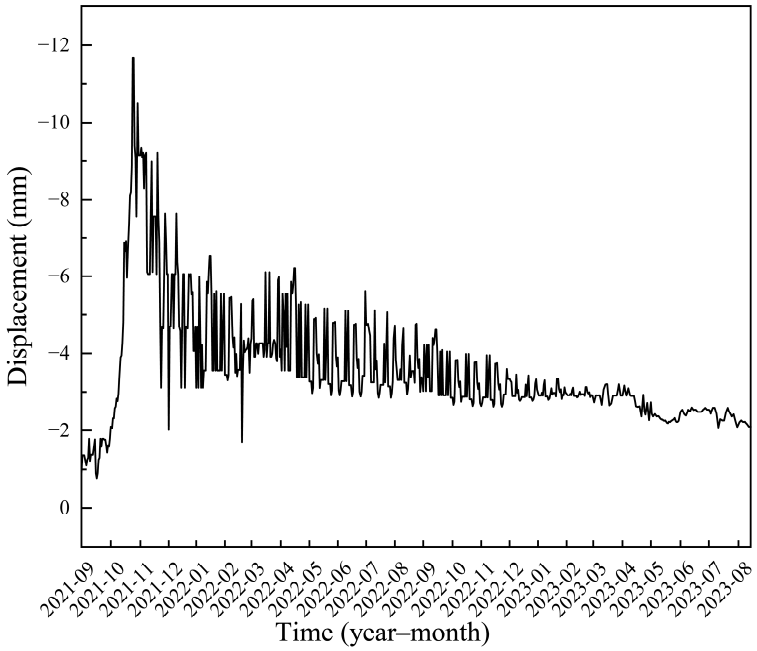


Figure 7. Monitoring data of pier displacement.

5. Discussion

5.1. Pile Shaft Axial Force

According to the monitoring data presented in Section 4.1, notable anomalies were identified at certain monitoring points of pile 3# between May and July 2021. During this period, short-term tensile stresses were recorded, as shown in Figure 8. In comparison, pile 14# exhibited no irregularities in stress measurements during the same timeframe. During this period, soil excavation was carried out on the channel side. At the same time, large concrete blocks were placed between the channel revetment and the pier cap to provide a stable roadbed for construction machinery. From a soil–structure interaction perspective, the observed tensile stresses indicate that Pile 3# transitioned from an active load-bearing element to a passive pile subjected to lateral soil movement. The placement of concrete blocks and the adjacent channel excavation created a significant asymmetric surcharge. In deep soft soil regions, such asymmetric loading induces substantial lateral plastic flow of the soil, which exerts lateral pressure on the pile shaft. The lateral earth pressure generated a bending moment, resulting in the recorded tensile stresses at the pile top. Unlike in stiff soil, where arching effects might mitigate load transfer, the rheological properties of soft soil facilitated the direct transfer of lateral thrust to the bridge foundation [48,49].

A significant increase in axial force was observed for pile 3# during mid to late June, as shown in Figure 8. The most pronounced change occurred at monitoring point F3-13, where the axial force rose abruptly from 100 kN to 961 kN before reducing to 157 kN. Site records indicate that this fluctuation coincided with a preloading operation conducted by the construction team on pile 3#. The abrupt surge in axial force confirms the high responsiveness to vertical preloading of the pile. The rapid reversion of the axial force suggests that the deformation remained largely elastic, preserving the structural integrity of the pile.

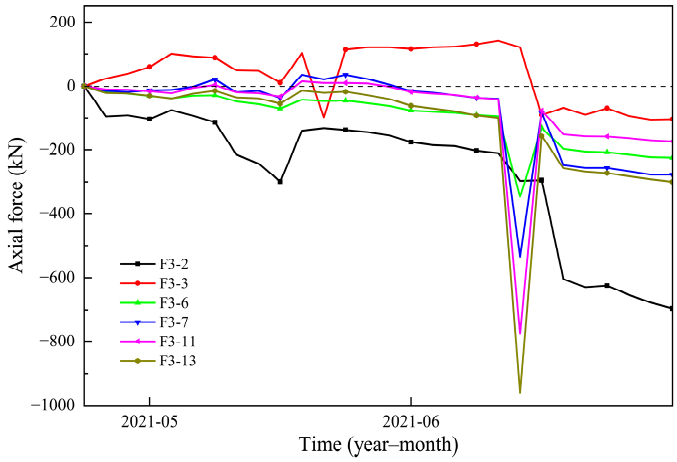
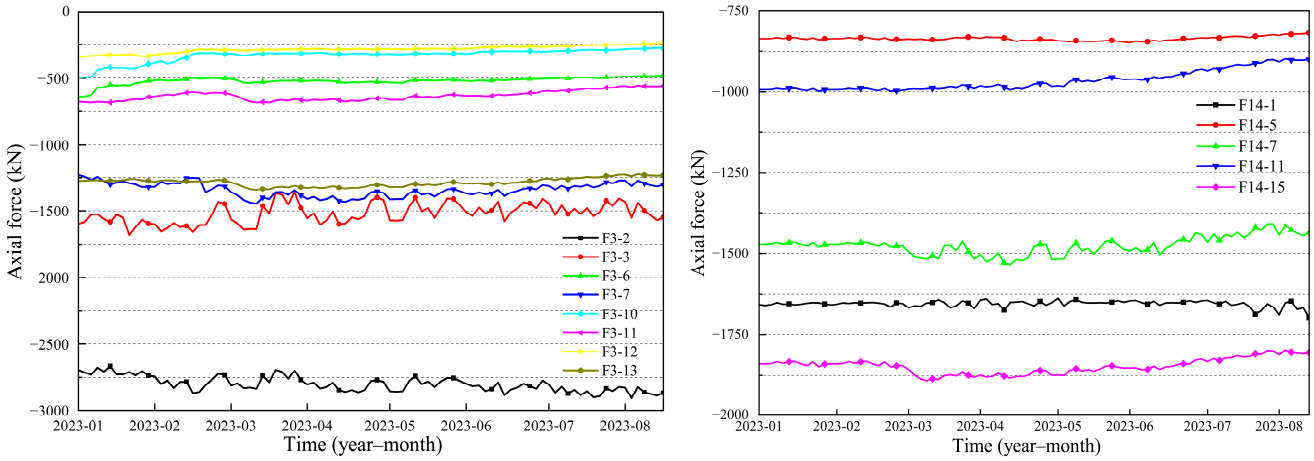


Figure 8. Monitoring data of the axial force of pile 3#.

As shown in Figure 9, the axial force growth rate at measurement point F3-2 exhibited a slight deceleration, while the axial forces at other measurement points for pile 3# and pile 14# showed a gradual decline in March 2023. On-site monitoring confirms that this specific timeframe corresponds to the start of water diversion into the channel. Crucially, the site was free from other external interferences during this period, with no activities such as surface surcharge, dewatering, or nearby mechanical operations taking place. The outward seepage from the channel resulted in increased soil moisture content around the piles and an elevated groundwater level. The rise in the groundwater table enhanced the pile buoyancy, which counteracted a portion of the vertical load [50]. Although the consolidation settlement of the soft soil induced negative skin friction (NSF) along the shafts of the rock-socketed piles, thereby increasing the pile axial force, the elevated groundwater table increased the pore water pressure in the surrounding soil. According to the effective stress principle, this reduced the effective stress and soil shear strength. Consequently, the NSF acting on the pile diminished, leading to a reduction in the axial force within the middle and lower sections of the pile. While the axial force at the pile head increased under the combined action of the superstructure load and NSF, the diminished NSF resulted in a decelerated rate of axial force accumulation [51,52].



(**a**) (**b**)

Figure 9. Monitoring data of axial force: (**a**) Axial force of pile 3# in 2023; (**b**) Axial force of pile 14# in 2023.

In the axial force monitoring data for pile 14#, the maximum axial force was recorded at measurement point F14-15, a behavior distinct from that observed in pile 3#. Analysis of the measurement locations indicates that F14-15 corresponds to the depth at which the pile

foundation is embedded into the rock layer. This phenomenon highlights the significance of the stiffness mismatch between the soft overburden and the underlying bedrock. At this rock-soil interface, the settlement of the soft soil generally exceeds the settlement of the stiff rock-socketed pile, resulting in significant NSF along the pile shaft. Consequently, the axial force at this point does not decrease with depth but rather increases to a maximum value. This indicates that the pile shaft at the rock interface must sustain not only the superstructure load but also the additional dragload derived from the settling soil.

5.2. Pile Inclination Angle

Based on the monitoring data presented in Section 4.2, monitoring point A3-7 exhibited a distinct tilting movement toward the channel between May and July 2021. In contrast, the remaining measuring points associated with pile 3# demonstrated tilting in the opposite direction, away from the channel during the same period. Similarly, the inclination angle data for pile 14# revealed that monitoring point A14-7 experienced the earliest and most significant change in inclination angle, recording the highest values among all monitoring points. The behavior of A3-7 and A14-7 deviated significantly from the overall deformation profile of the piles, suggesting a unique response to external conditions. This divergence is fundamentally controlled by the stratigraphy, specifically the geological context of these points. Both A3-7 and A14-7 are located within the mid-section of the soft soil layer, an area characterized by suboptimal engineering properties and high compressibility. This phenomenon reveals that the thick soft soil layer acts as an amplification zone for deformation. These points within the weak soil layer are highly susceptible to variations in soil pressure and lateral displacements transmitted from the upper portion of the pile. Consequently, due to the lack of effective elastic support from the surrounding soil, their heightened sensitivity resulted in more pronounced deviations compared to other monitoring points.

5.3. Bridge Pier Displacement

According to the pier displacement monitoring data presented in Section 4.3, the pier exhibited notable lateral displacement toward the channel, peaking at 12.5 mm on October 24. Given the rigid connection among the pier, pile cap, and pile head, the observed displacement is equivalent to the displacement of the pile head. As stipulated in the Technical Code for Building Pile Foundations (JGJ94-2008) [53], structural stability may be compromised if the pile head displacement exceeds 10 mm. Consequently, the recorded displacement surpassed this critical threshold, indicating a potential risk to the structural safety. Site investigations revealed that channel revetment construction was ongoing during this period. Excavation activities were conducted proximal to the pile cap, with a depth of 2 m in the symmetrical unloading area. This depth was significantly shallower than the channel depth of 8 m, as depicted in Figure 10. Moreover, a 3 m-high soil stockpile was observed approximately 10 m from the pile cap, exerting additional surcharge loads and lateral pressure on the structure. Upon identifying this critical condition, immediate remedial measures were implemented. These measures included expanding the unloading area, increasing the excavation depth, and removing the stockpiled soil. Following these countermeasures, subsequent monitoring data indicated that the displacement stabilized within acceptable limits, thereby mitigating the risk to the structural stability.



Figure 10. Photos of the excavation site of soil in the area away from the channel side.

To examine the influence of soil accumulation and symmetric excavation on the displacement of the bridge pier, a finite element model was developed using Abaqus to simulate excavation adjacent to the pier, as shown in Figure 11. The model dimensions were set at 200 m in length, 100 m in width, and 100 m in height. The distance from the boundaries to the piles significantly exceeds five times the excavation depth. The boundary condition of the model includes fixed horizontal displacements for all lateral boundaries, but allows for free vertical displacements. The displacement of the model's bottom plane is completely fixed, and there is no displacement restriction on the top plane. The modified Cambridge model was adopted to represent the mechanical behavior of silty clay and muddy clay. For the soft soil layers, a normally consolidated state was assumed. Consequently, the initial yield surface parameter was initialized as one-half of the in situ effective overburden pressure calculated from the soil self-weight. Referring to the study by Yu et al. [54] on the modified Cambridge model parameters for soft soils in the Hangjiahu alluvial-lacustrine plain, the constitutive parameters used for the soft soil layers in this simulation are listed in Table 2. For the silt and moderately weathered bedrock, the Mohr-Coulomb criterion was adopted to characterize their mechanical response. The specific parameters are summarized in Table 1. The concrete components, including piles, caps, and piers, were simulated as linear elastic materials with a density of 2460 kg/m^3, an Elastic modulus of 30,000 MPa, and a Poisson's ratio of 0.2. The interaction between the structure and the surrounding soil was simulated using the surface-to-surface contact pair algorithm. Hard contact was specified for the normal behavior, while the penalty friction formulation was adopted to characterize the shear behavior. The C3D8R element type was used to analyze both the soil response and the structural behavior of the pier. A graded meshing technique was employed to optimize computational efficiency while maintaining numerical accuracy. The mesh density was increased in key areas such as the piers and piles, where the minimum element size was set to 0.9 m, while a coarser mesh was used in far-field areas. The model consists of 84,859 elements in total. Before the simulation, strict mesh quality verifications were performed in ABAQUS to minimize numerical errors, covering shape metrics and analysis checks. To simulate the effects of the superstructure, a pressure load representing the superstructure load of the bridge was applied at the top of the pier. Soil accumulation was modeled as an external pressure applied within the loading area, positioned 10 m from the pier, with a total load of 4650 kN. Symmetric excavation and channel excavation were simulated using the model change feature in Abaqus, where elements within these zones were deactivated. The unloading area was defined with dimensions of 30 m in length, 10 m in width, and 3.5 m

in depth. Specifically, to align with the actual on-site construction scheme, the channel excavation was executed in two distinct analysis steps. The first excavation step involved a depth of 3.5 m, followed by a second step with an excavation depth of 4.5 m. It should be noted that the symmetric excavation was performed simultaneously with the first stage of the channel excavation. Since the excavation was completed rapidly relative to the consolidation time of the soft clay, the excavation steps were simulated as an undrained analysis to capture the most critical stability conditions. Four distinct scenarios were formulated by combining soil accumulation and symmetric excavation, as shown in Table 3. The displacement of the pier under these varying conditions was analyzed to assess the individual and combined effects of soil accumulation and symmetric excavation.

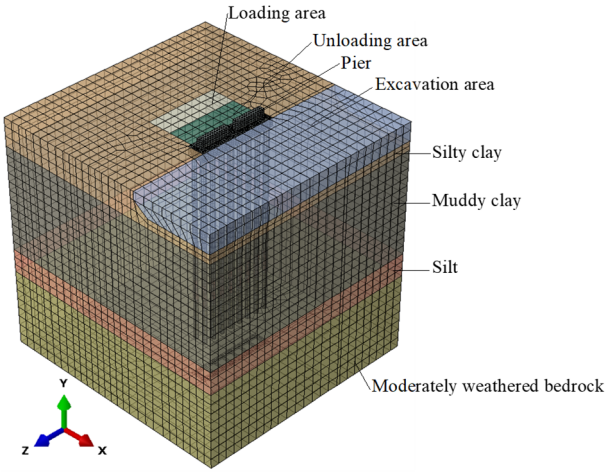


Figure 11. Finite element model.

Table 2. Parameters of modified Cambridge model of soil layer.

Soil Type	λ	κ	M	e_0
Silty clay	0.038	0.012	1.123	0.967
Muddy clay	0.050	0.021	1.076	1.712

Table 3. Simulated scenarios for soil accumulation and symmetrical excavation.

Case	Simulated Scenarios
1	No soil accumulation, symmetric excavation
2	No soil accumulation, no symmetric excavation
3	Soil accumulation, symmetric excavation
4	Soil accumulation, no symmetric excavation

Figure 12 shows the displacement of the pier in the direction perpendicular to the channel for four cases. The peak displacements recorded at the pier top for Cases 1 through 4 are 6.5 mm, 9.3 mm, 7.9 mm, and 12.2 mm, respectively. The results align well with the findings of Bao et al. [55], where a maximum excavation-induced pier displacement of 7.2 mm was reported under similar geological conditions. The displacements observed in Case 1 and Case 3 demonstrate strong consistency with these literature observations, thereby validating the fidelity of the finite element model. In contrast, Case 4 yielded a larger displacement of 12.2 mm, which is attributed to the presence of surcharge loading and asymmetric excavation. This outcome approximates the field monitoring values, further corroborating the simulation accuracy and highlighting the adverse impact of surcharge loading and asymmetric excavation on bridge stability. As depicted in Figure 12a,b,

in the absence of soil accumulation, the pier top displacement under symmetric excavation decreases by 2.8 mm compared to the case without symmetric excavation. Similarly, when soil accumulation is present, the pier top displacement under symmetric excavation is reduced by 4.3 mm relative to the non-symmetric excavation, as shown in Figure 12c,d. Furthermore, under symmetric excavation conditions, the pier top displacement without soil accumulation is 1.4 mm lower than that observed with soil accumulation, as demonstrated in Figure 12a,c. In the absence of symmetric excavation, the pier top displacement without soil accumulation is 2.9 mm less than that with soil accumulation, as shown in Figure 12b,d. The removal of soil accumulation results in a 23.8% reduction in pier top displacement, while symmetric excavation contributes to a 35.2% reduction. This can be attributed to the closer proximity of the unloading area to the pier compared to the loading area. These results underscore the substantial adverse effects of soil accumulation and the asymmetric excavation on pier displacement.

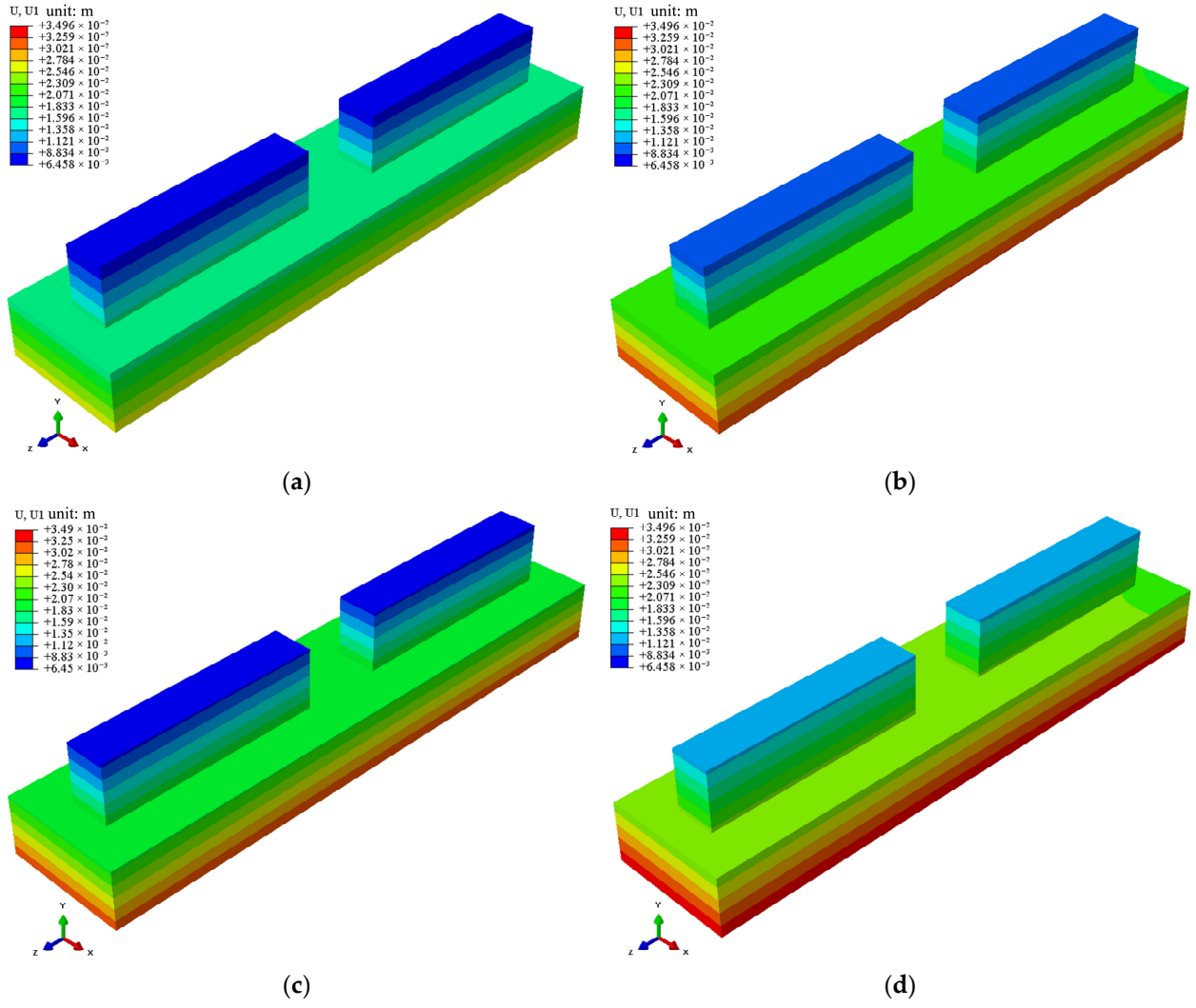


Figure 12. Displacement of pier in the direction perpendicular to the channel: (**a**) Case 1; (**b**) Case 2; (**c**) Case 3; (**d**) Case 4.

6. Conclusions

This study presented a comprehensive long-term monitoring analysis to evaluate the stress and deformation behavior of bridge pile foundations during the simultaneous construction of a bridge and an adjacent channel. The investigation focused on assessing the impact of construction activities on the structural stability of the bridge pile foundation.

Additionally, abnormal phenomena identified during the monitoring process are critically analyzed. In response to potential safety risks, appropriate mitigation measures were promptly proposed. The main findings of the study are summarized as follows:

1. The axial force in the pile reached its maximum at the pile head and exhibits a gradual reduction with increasing depth, consistent with the typical distribution pattern observed in friction piles. However, within the rock-socketed section, the relative displacement between the pile and the surrounding soil diminished, leading to the accumulation of dragload and a localized increase in the axial force.
2. Upon the filling of the channel with water, infiltration into the adjacent soil occurred, leading to an increase in soil moisture content. The rising groundwater table increased buoyancy while simultaneously reducing NSF, which collectively decreased the axial force of the pile.
3. Soil excavation substantially influenced the inclination angle of the pile body, with the effect being particularly pronounced in the mid-section of the soft soil layer. This depth acted as an amplification zone for deformation due to strain localization and the lack of lateral confinement. This observation indicates that pile foundations in soft soil are highly susceptible to plastic flow and instability under external loading and soil disturbances.
4. Asymmetric soil excavation and surcharge loads significantly influenced pier displacement by transforming the foundation into a passive pile, thereby compromising the structural stability of the bridge. This underscores the critical need for meticulous management of excavation processes and load distribution during construction to mitigate potential risks. Practical solutions such as enforcing a strict safety setback distance for machinery, real-time monitoring of pore water pressure, and avoiding asymmetric excavation are recommended.

Author Contributions: Conceptualization, W.D. and S.W.; methodology, W.D.; software, W.D.; validation, W.D. and S.W.; formal analysis, W.D. and G.W.; investigation, W.D., W.H. and J.L.; resources, W.D. and S.W.; data curation, W.D. and G.W.; writing—original draft preparation, W.D.; writing—review and editing, S.W.; visualization, W.D.; supervision, S.W.; project administration, S.W.; funding acquisition, W.D. and S.W. All authors have read and agreed to the published version of the manuscript.

Funding: This research was funded by the National Earthquake Science Joint Foundation of China (Grant No. U1939209), the Key Program of National Natural Science Foundation of China (Grant No. 42330704), the Science and Technology Plan Project of Department of Transportation of Zhejiang Province (Grant No. 2021038), and the Postgraduate Research and Practice Innovation Program of Jiangsu Province (Grant No. KYCX24_1581).

Data Availability Statement: The data that support the findings of this study are available from the corresponding author upon reasonable request.

Conflicts of Interest: The authors declare no conflicts of interest.

References

1. Namazi, E.; Mohamad, H.; Hajihassani, M. 3D behaviour of buildings due to tunnel induced ground movement. *Transp. Geotech.* **2021**, *31*, 10661. [CrossRef]
2. Wu, Y.; Hao, R.; Zhang, T.; Huang, D.; Xiong, Z. Experimental and numerical study on the impact of multi-line TBM tunneling in fractured zones on building deformation. *Buildings* **2025**, *15*, 3322. [CrossRef]
3. Zhang, X.; Zhao, D.; Shi, X.; Gao, X.; Zhang, Y.; Wang, S. Investigation into the impacts of cover-and-cut top-down metro station construction on adjacent buildings: A case study. *Buildings* **2025**, *15*, 4149. [CrossRef]
4. Mao, Z.; Ding, T.; Hu, F.; Ye, S.; Ding, L.; Shu, R.; Zhang, X.; Song, M. The deformation characteristics and patterns of adjacent existing metro structures caused by foundation pit excavation under different support forms. *Buildings* **2025**, *15*, 4178. [CrossRef]

5. Richards, P.W.; Rollins, K.M.; Stenlund, T.E. Experimental testing of pile-to-cap connections for embedded pipe piles. *J. Bridge Eng.* **2011**, *16*, 286–294. [CrossRef]
6. Matsumoto, K.; Panting, C.A.L.; Kitratporn, N.; Takeuchi, W.; Nagai, K.; Iwasaki, E. Performance assessment using structural analysis and spatial measurement of a damaged suspension bridge: Case study of Twantay bridge, Myanmar. *J. Bridge Eng.* **2018**, *23*, 05018008. [CrossRef]
7. Bi, J.; Wang, G.; Mu, W.; Wen, H.; Pei, W.; Zhang, Q.; Yang, S.; Mao, M.; Lin, G.; Wang, C. A matrix for estimating the unfrozen water content of freezing soils. *CATENA* **2025**, *256*, 109050. [CrossRef]
8. Zhang, L.; Zhang, P.; Xu, D.; Zhou, T. Seismic damage analysis of piled pier system constructed on soft clay ground. *J. Bridge Eng.* **2021**, *26*, 04020133. [CrossRef]
9. Tian, N.; Li, M.; Huang, Q.; Yang, X.; Sun, Y.; Chen, J. Deformation response of underlying twin shield tunnels induced by large excavation in soft soils. *Buildings* **2025**, *15*, 4023. [CrossRef]
10. Zheng, X.; Wang, X.; Shen, K.; Gu, X. Determination of HSS model parameters for soft clays in Hangzhou: Statistical analysis and engineering validation. *Buildings* **2025**, *15*, 3886. [CrossRef]
11. Liu, Y.; Chen, Q.; Chen, X.; Liao, C. Seismic damage mechanism of five-story and three-span underground complex in soft soil site. *Buildings* **2025**, *15*, 2380. [CrossRef]
12. Finno, R.J.; Blackburn, J.T.; Roboski, J.F. Three-dimensional effects for supported excavations in clay. *J. Geotech. Geoenvironmental Eng.* **2007**, *133*, 30–36. [CrossRef]
13. Zhao, W.; Du, C.; Sun, L.; Chen, X. Field measurements and numerical studies of the behaviour of anchored sheet pile walls constructed with excavating and backfilling procedures. *Eng. Geol.* **2019**, *259*, 105165. [CrossRef]
14. Bi, J.; Pan, Y.; Mu, W.; Yang, S.; Wang, G.; Mao, M.; Wang, S.; Wei, T. Predicting the unfrozen water content of freezing soils using an artificial neural network model. *J. Cold Reg. Eng.* **2026**, *40*, 04025050. [CrossRef]
15. Shi, J.; Wei, J.; Ng, C.W.W.; Lu, H.; Ma, S.; Shi, C.; Li, P. Effects of construction sequence of double basement excavations on an existing floating pile. *Tunn. Undergr. Space Technol.* **2022**, *119*, 104230. [CrossRef]
16. Mukherjee, S.; Kumar, J. Stability analysis of a vertical excavation reinforced with horizontal nails using three-dimensional finite elements limit analysis. *Transp. Geotech.* **2024**, *44*, 101168. [CrossRef]
17. Ashour, M.; Abbas, A.I.; Boskovic, S. Pile cap interaction with bridge pile foundations under lateral loads. *J. Bridge Eng.* **2019**, *24*, 04019053. [CrossRef]
18. Rezvani, R.; Tutunchian, M.A. Horizontal displacement of urban deep excavated walls supported by multistrands anchors, steel piles, and in situ concrete piles: Case study. *Int. J. Geomech.* **2021**, *21*, 05020008. [CrossRef]
19. Yang, Y.; Li, J.; Liu, C.; Ma, J.; Zheng, S.; Chen, W. Influence of deep excavation on adjacent bridge piles considering underlying karst cavern: A case history and numerical investigation. *Acta Geotech.* **2022**, *17*, 545–562. [CrossRef]
20. Mo, P.; Marshall, A.M.; Fang, Y. Cavity expansion–contraction-based method for tunnel–soil–pile interaction in a unified clay and sand model: Drained analysis. *Int. J. Geomech.* **2021**, *21*, 04021055. [CrossRef]
21. Lu, H.; Shi, J.; Ng, C.W.W.; Lv, Y. Three-dimensional centrifuge modeling of the influence of side-by-side twin tunneling on a piled raft. *Tunn. Undergr. Space Technol.* **2020**, *103*, 103486. [CrossRef]
22. Fan, Y.; Cai, J.; Wang, J. An analytical method evaluating the evolution of group effect for vertically loaded pile groups subjected to tunnel excavation. *Appl. Sci.* **2023**, *13*, 517. [CrossRef]
23. Liu, X.; Liu, Y.; Qu, W.; Tu, Y. Internal force calculation and supporting parameters sensitivity analysis of side piles in the subway station excavated by Pile-Beam-Arch method. *Tunn. Undergr. Space Technol.* **2016**, *56*, 186–201. [CrossRef]
24. Faheem, H.; Cai, F.; Ugai, K.; Hagiwara, T. Two-dimensional base stability of excavations in soft soils using FEM. *Comput. Geotech.* **2003**, *30*, 141–163. [CrossRef]
25. Bal, A.R.L.; Dang, T.S.; Meschke, G. A 3D particle finite element model for the simulation of soft soil excavation using hypoplasticity. *Comput. Part. Mech.* **2020**, *7*, 151–172. [CrossRef]
26. Li, G.; Qin, F.; Yan, N.; Qiao, X.; Si, L.; Zhao, S. Surface deformation characteristics and influencing factors in deep foundation pit excavations for subway projects in Ningbo's soft soil area. *Buildings* **2025**, *15*, 1229. [CrossRef]
27. Feng, W.; Xu, J.; Zhang, R.; Yan, Z.; Fu, L.; Zhu, Y.; Zhang, G.; Chen, Z. Study on excavation response of metro station foundation pit in water-bearing strata adjacent to tall buildings. *Buildings* **2025**, *15*, 3982. [CrossRef]
28. Xu, J.; Deng, H.; Liu, Z.; Dai, G.; Ke, L.; Guo, X.; Zhang, Z. Protection of low-strength shallow-founded buildings around deep excavation: A case study in the Yangtze River soft soil area. *Buildings* **2025**, *15*, 4094. [CrossRef]
29. Blackburn, J.T.; Finno, R.J. Three-dimensional responses observed in an internally braced excavation in soft clay. *J. Geotech. Geoenviron. Eng.* **2016**, *133*, 1364–1373. [CrossRef]
30. Liang, Y.; Liu, N.; Yu, F.; Gong, X.; Chen, Y. Prediction of response of existing building piles to adjacent deep excavation in soft clay. *Adv. Civ. Eng.* **2019**, *2019*, 8914708. [CrossRef]
31. Choosrithong, K.; Schweiger, H.F. Numerical investigation of sequential strut failure on performance of deep excavations in soft soil. *Int. J. Geomech.* **2020**, *20*, 04020063. [CrossRef]

32. Chen, S.; Cui, J.; Liang, F. Case study on the deformation coupling effect of a deep foundation pit group in a coastal soft soil area. *Appl. Sci.* **2022**, *12*, 6205. [CrossRef]
33. Yang, Y.; Chen, C.; Liu, C.; Huang, L.; Chen, W.; Lin, N.; Cui, J.; Xie, W. Performance of a deep excavation and the influence on adjacent piles: A case history in karst region covered by clay and sand. *Undergr. Space* **2023**, *8*, 45–60. [CrossRef]
34. Li, H.; Liu, S.; Tong, L. Evaluation of lateral response of single piles to adjacent excavation using data from cone penetration tests. *Can. Geotech. J.* **2019**, *56*, 236–248. [CrossRef]
35. Li, Y.; Zhang, W.; Jiang, N.; Li, H. Surface settlement damage model of pile-anchor supporting structure in deep excavation. *Adv. Civ. Eng.* **2020**, *2020*, 1907526. [CrossRef]
36. Yamashita, K.; Yamada, T.; Hamada, J. Investigation of settlement and load sharing on piled rafts by monitoring full-scale structures. *Soils Found.* **2011**, *51*, 513–532. [CrossRef]
37. Stepanov, M.A.; Volosyuk, D.V.; Bartolomey, L.A. Geotechnical monitoring results of 22-storey buildings on combined strip pile foundations with prestressed soil bases. *J. Phys. Conf. Ser.* **2021**, *1928*, 012027. [CrossRef]
38. Fellenius, B.H.; Kim, S.R.; Chung, S.G. Long-term monitoring of strain in instrumented piles. *J. Geotech. Geoenvironmental Eng.* **2009**, *135*, 1583–1595. [CrossRef]
39. Nguyen, V.D.; Luo, Q.; Wang, T.; Zhang, L.; Zhan, Y.; Nguyen, T.P. Monitoring of an instrumented geosynthetic-reinforced piled embankment with a triangular pile configuration. *Int. J. Rail Transp.* **2023**, *11*, 69–91. [CrossRef]
40. Chen, Z.; Zhang, N.; Zhang, X. Settlement monitoring system of pile-group foundation. *J. Cent. South Univ. Technol.* **2011**, *18*, 2122–2130. [CrossRef]
41. Kister, G.; Winter, D.; Gebremichael, Y.M.; Leighton, J.; Badcock, R.A.; Tester, P.D.; Krishnamurthy, S.; Boyle, W.J.O.; Grattan, K.T.V.; Fernando, G. Methodology and integrity monitoring of foundation concrete piles using Bragg grating optical fibre sensors. *Eng. Struct.* **2007**, *29*, 2048–2055. [CrossRef]
42. Mohamad, H.; Soga, K.; Pellew, A.; Bennett, P.J. Performance monitoring of a secant-piled wall using distributed fiber optic strain sensing. *J. Geotech. Geoenvironmental Eng.* **2011**, *137*, 1236–1243. [CrossRef]
43. Guo, Z.; Zhao, Z. Application of distributed optical fiber sensing technique in pile foundation monitoring. *IOP Conf. Ser. Earth Environ. Sci.* **2018**, *189*, 052074. [CrossRef]
44. Liu, F.; Xu, Q.; Liu, Y. Condition diagnosis of long-span bridge pile foundations based on the spatial correlation of high-density strain measurement points. *Sustainability* **2021**, *13*, 12498. [CrossRef]
45. Klar, A.; Bennett, P.J.; Soga, K.; Mair, R.J.; Tester, P.; Fernie, R.; St John, H.D.; Torp-Peterson, G. Distributed strain measurement for pile foundations. *Proc. Inst. Civ. Eng. Geotech. Eng.* **2006**, *159*, 135–144. [CrossRef]
46. Momeni, E.; Poormoosavian, M.; Tehrani, H.S.; Fakher, A. Reliability analysis and risk assessment of deep excavations using random-set finite element method and event tree technique. *Transp. Geotech.* **2021**, *29*, 100560. [CrossRef]
47. Lai, V.; Kounlavong, K.; Keawsawasvong, S.; Banyong, R.; Wipulanusat, W.; Jamsawang, P. Undrained basal stability of braced circular excavations in anisotropic and non-homogeneous clays. *Transp. Geotech.* **2023**, *39*, 100945. [CrossRef]
48. Poulos, H.G.; Chen, L.T. Pile response due to excavation-induced lateral soil movement. *J. Geotech. Geoenvironmental Eng.* **1997**, *123*, 94–99. [CrossRef]
49. Ong, D.E.; Leung, C.E.; Chow, Y.K. Pile behavior due to excavation-induced soil movement in clay. I: Stable wall. *J. Geotech. Geoenvironmental Eng.* **2006**, *132*, 36–44. [CrossRef]
50. Fan, Z.; Xu, C.; Yang, K.; Xue, X.; Zeng, C. Experimental study on the influence of rising water levels on the buoyancy of building structure. *Water* **2025**, *17*, 1377. [CrossRef]
51. Zhang, Y.; Zhou, L.; Wang, M.; Ding, X.; Wang, C. Experimental study on the negative skin friction of the pile group induced by rising and lowering the groundwater level. *Adv. Civ. Eng.* **2021**, *2021*, 2574727. [CrossRef]
52. Chalajour, S.; Blatz, J.A. Assessment of the unified design method for piles subjected to negative skin friction using field studies and numerical modeling. *Can. Geotech. J.* **2025**, *62*, 1–17. [CrossRef]
53. *JGJ94-2008*; Technical Code for Building Pile Foundations. Ministry of Housing and Urban-Rural Development of the People's Republic of China: Beijing, China; China Architecture & Building Press: Beijing, China, 2008.
54. Yu, H.; Chen, X.; Yi, L.; Qiu, J.; Gu, Z.; Zhao, H. Parameter inversion and application of soft soil modified Cambridge model. *Rock Soil Mech.* **2023**, *44*, 3318–3326. (In Chinese) [CrossRef]
55. Bao, X.; Cheng, Z.; Lv, C.; Shen, J.; Chen, X.; Cui, H. Analysis of the influence of deep foundation excavation on adjacent viaduct pile foundation considering train dynamic loads. *Appl. Sci.* **2023**, *13*, 1572. [CrossRef]

Disclaimer/Publisher's Note: The statements, opinions and data contained in all publications are solely those of the individual author(s) and contributor(s) and not of MDPI and/or the editor(s). MDPI and/or the editor(s) disclaim responsibility for any injury to people or property resulting from any ideas, methods, instructions or products referred to in the content.